HHS Public Access

Author manuscript

Neuron. Author manuscript; available in PMC 2016 June 20.

Published in final edited form as:

Neuron. 2014 October 1; 84(1): 214–226. doi:10.1016/j.neuron.2014.08.019.

Descending control of neural bias and selectivity in a spatial attention network: rules and mechanisms

Shreesh P. Mysore[*,†] and **Eric I. Knudsen**

Department of Neurobiology, Stanford University, 299 W. Campus Drive, Stanford CA 94305, USA

SUMMARY

The brain integrates stimulus-driven (exogenous) activity with internally generated (endogenous) activity to compute the highest priority stimulus for gaze and attention. Little is known about how this computation is accomplished neurally. We explored the underlying functional logic in a critical component of the spatial attention network, the optic tectum (OT, superior colliculus in mammals), in awake barn owls. We found that space-specific endogenous influences, evoked by activating descending forebrain pathways, bias competition among exogenous influences, and substantially enhance the quality of the categorical neural pointer to the highest priority stimulus. These endogenous influences operate across sensory modalities. Biologically grounded modeling revealed that the observed effects on network bias and selectivity require a simple circuit mechanism: endogenously driven gain modulation of feedback inhibition among competing channels. Our findings reveal fundamental principles by which internal and external information combine to guide selection of the next target for gaze and attention.

INTRODUCTION

The ability of animals to behave adaptively in complex environments depends critically on their selecting and preferentially processing the most important information at each instant. Both stimulus-driven exogenous influences and internally generated endogenous influences exert control over this essential capacity, called attention. Studies of attention have focused largely on the effects of selection on sensory processing: Behavioral studies have demonstrated increases in performance to stimuli that have been selected as the target of attention and decreases in performance associated with unattended stimuli (Carrasco, 2011; Treisman, 1964). In parallel, electrophysiological and functional imaging studies have demonstrated increases in neural activity and synchrony in response to stimuli that have been selected as the target of attention and decreases in neural activity in response to unattended stimuli (Carrasco, 2011; Maunsell and Treue, 2006; Reynolds and Chelazzi,

[*] Correspondence to: shreesh.mysore@jhu.edu.

[†] Current Address: Department of Psychological and Brain Sciences, Johns Hopkins University, 3400 N. Charles Street, Ames Hall, Baltimore MD 21218

Author contributions SPM and EIK designed the research and wrote the paper. SPM performed the experiments and the analyses.

Supplementary information accompanies the paper.

2004). Little is known, however, about the rules and circuit mechanisms by which the brain determines, in the first place, which stimulus, among all potential stimuli, is the highest priority stimulus for attention. Here, we reveal and explore some of these rules and mechanisms.

An ideal site in the brain to study this question is the midbrain stimulus selection network, which comprises the OT (or superior colliculus, SC, in mammals) and several interconnected nuclei in the midbrain tegmentum. The SC/OT integrates exogenous and endogenous information into a topographic map of space (Knudsen, 2011; Wallace and Stein, 1996). Neurons in the SC/OT respond with higher firing rates to stimuli of higher physical salience (such as greater strength or speed of motion) (Knudsen, 2011; Wurtz and Albano, 1980), while not being systematically tuned for the features of the stimuli (Horwitz and Newsome, 1999; Li et al., 1996). Their responses are also modulated by endogenous signals (Goldberg and Wurtz, 1972; Ignashchenkova et al., 2004). Moreover, multiple lines of evidence demonstrate a role for the SC/OT in target selection for attention: Inactivation of the intermediate and deep layers of the SC (SCid) in behaving monkeys severely impairs the selection of targets among distracters when selection is controlled by either exogenous or endogenous influences (Lovejoy and Krauzlis, 2010; McPeek and Keller, 2004; Zenon and Krauzlis, 2012). Conversely, focal electrical microstimulation applied to the SCid improves the ability of monkeys to detect and discriminate visual stimuli specifically at the spatial location represented by the microstimulation site (Carello and Krauzlis, 2004; Cavanaugh and Wurtz, 2004; Muller et al., 2005).

Past work in barn owls has examined parametrically the way in which the midbrain network represents the strongest stimulus among competing stimuli (Asadollahi et al., 2010; Mysore et al., 2011). Neurons in the OTid are highly sensitive to the physical salience of the stimulus inside their receptive fields *relative to* the physical salience of stimuli at any other location. They fire strongly only when their receptive field stimulus is the strongest stimulus, and do so independently of the absolute strengths of the stimuli. As a result, OTid neurons provide, as a population, a binary-like representation of the strongest stimulus (Mysore and Knudsen, 2011). Computational modeling has revealed that the most efficient neural circuit to implement such flexible, binary-like signaling is reciprocal inhibition of feedforward lateral inhibition (Mysore and Knudsen, 2012), a circuit that has now been shown to exist within the midbrain selection network (Goddard et al., 2014).

Here, we explore how evoked, space-specific influences from the forebrain alter stimulus-driven competition in the midbrain network to shape its computation of the highest priority stimulus. Through computational modeling, we also identify a fundamental circuit mechanism that is essential for these critical computations.

RESULTS

Exogenous stimuli were presented to passive, awake barn owls following a specialized experimental protocol, called the “competition protocol” (Mysore et al., 2011), that measures quantitatively and parametrically the neural representation of relative stimulus priority (Fig. 1A). Two stimuli were presented simultaneously: one was presented inside a

recorded neuron's receptive field (“RF stimulus”) and was held at a fixed strength; the other was presented far outside the receptive field (> 30° away in the same hemifield; “competitor”) and its strength was parametrically varied from being weaker to stronger than the RF stimulus. The RF stimulus was always a looming visual dot, its strength being controlled by its loom speed and measured in degrees/s, while the competitor was either a visual looming dot or an auditory broadband noise burst, the strength of the latter being controlled by its amplitude and measured in dB.

In order to evoke space-specific endogenous influences, we took advantage of the tight coupling that exists between gaze control and the redirection of spatial attention. In humans, saccadic shifts of gaze are always preceded by covert shifts of spatial attention to the location of the impending gaze shift (Deubel and Schneider, 1996; Hoffman and Subramaniam, 1995; Kowler et al., 1995). In monkeys, electrical microstimulation in the forebrain gaze control area (frontal eye field; FEF), with currents below those necessary to elicit an eye saccade (“sub-saccadic” currents), improves behavioral detection of stimuli at the location represented by the stimulation site (Moore and Fallah, 2001) and increases the responsiveness of cortical neurons to stimuli at the corresponding location (Moore and Armstrong, 2003). These effects are indistinguishable from those that occur during voluntary shifts of spatial attention (Armstrong and Moore, 2007). Consequently, electrical microstimulation of the FEF has been used routinely in monkeys to evoke space-specific endogenous influences (Clark et al., 2011). In owls, the arcopallial gaze field (AGF) shares functional and anatomical characteristics with the primate FEF: electrical microstimulation of the AGF evokes saccadic changes in gaze direction (Bruce et al., 1985; Knudsen et al., 1995); sub-saccadic electrical microstimulation causes space-specific modulation of sensory neural responsiveness (Moore and Armstrong, 2003; Winkowski and Knudsen, 2006); the AGF plays a necessary role in working memory-dependent gaze control (Dias and Segraves, 1999; Knudsen and Knudsen, 1996); and it exhibits similar patterns of anatomical projections to sensorimotor and premotor structures, including direct projections to the OTid/SCid (Knudsen et al., 1995; Stanton et al., 1988). Therefore, we used sub-saccadic electrical microstimulation of the AGF (Experimental Procedures) to study the effects of space-specific endogenous influences on stimulus competition in the midbrain selection network (Mysore and Knudsen, 2013; Winkowski and Knudsen, 2006).

The effects we report of electrically microstimulating the AGF most likely result from the activation of the strong and direct projections from the AGF to the midbrain network (Knudsen et al., 1995). In addition, AGF microstimulation may have also activated indirect descending pathways from the forebrain (Knudsen, 2011), and these alternate pathways may have contributed to the observed effects. However, confounding effects caused by antidromic activation of OT neurons can be ruled out because the OT does not project directly to the AGF.

Effects of spatially congruent AGF microstimulation on the encoding of the highest priority stimulus

First, we examined the effects of AGF microstimulation on stimulus competition in the OTid when the microstimulation was delivered to a site in the AGF that encoded the same location

(within 5°; Winkowski and Knudsen, 2006) as the receptive field of the recorded OTid neuron (Fig. 1A). This configuration, referred to as “aligned microstimulation”, results in the endogenous influence being congruent with the location of the RF stimulus.

Previously (Mysore et al., 2011), we have shown that OTid neurons, when tested with the competition protocol, exhibit a systematic decrease in firing rates with increasing strength of the competitor stimulus, a profile of responses referred to collectively as the competitor strength-response profile or CRP. In that study, we showed that high response rates within the CRP indicate that the RF stimulus is the stronger stimulus while low response rates indicate that the RF stimulus is the weaker stimulus. On average, the midpoint of the transition from high to low responses represents the point at which the RF and competitor stimuli are equal in strength (for instance, equal loom speeds) (Mysore et al., 2011). The more gradual the transition from high to low response rates, the greater the ambiguity in the signaling of the stronger stimulus when the competing stimuli are very close in strength.

Consistent with these previous results, the CRP for the neuron illustrated in Figure 1B,C exhibited a gradual transition from high to low response rates as the strength of the competitor increased (Fig. 1C, black: r=-0.8, p=0.014, correlation test). It was well-fit (r^2=0.81) by a standard sigmoidal function with four parameters: the steady-state minimum firing rate, the steady-state maximum firing rate, the strength of the competitor at which responses to the RF stimulus were midway (50%) between minimum and maximum (s_{50}), and the maximum slope (Experimental Procedures).

Randomly interleaved with these trials in which no microstimulation was applied were trials in which microstimulation was delivered to an aligned site in the AGF (aligned with the OTid RF). Aligned AGF microstimulation produced two key changes in the CRP (Fig. 1B,C, red). First, the CRP shifted rightward to favor the RF stimulus (increase in the s_{50}: Wald F-test, $F_{1,5}$=15.9, p=0.01; Experimental Procedures). Second, the maximum slope of the CRP increased, indicating a sharper transition from maximum to minimum firing rates with increasing competitor strength (Wald F-test, $F_{1,5}$=10.3, p=0.024; Experimental Procedures). This effect was quantified as a narrowing of the “transition range” (Mysore et al., 2011): the range of competitor strengths over which CRP responses dropped by 90% of the maximum change (Fig. 1C, shaded areas; Experimental Procedures). The effects of AGF microstimulation were consistent across a population of OTid neurons (Fig. 1DE and Fig. S1E). Thus, aligned AGF microstimulation shifted CRPs rightward to favor the representation of the congruent RF stimulus and produced sharper transitions in the response rates with increasing competitor strength, while having little or no effect on minimum or maximum response rates. These effects of aligned AGF microstimulation on OTid responses to *competing* stimuli could not have been predicted from its effects on OTid responses to *single* stimuli (response increases, (Winkowski and Knudsen, 2006)).

The effects of AGF microstimulation were not specific to competition among visual stimuli. We obtained similar results when we used an auditory noise burst as the competitor stimulus, (Fig. S1A-D,F). Thus, the effects of aligned AGF microstimulation on stimulus-driven competition generalize across sensory modalities of the competing stimuli.

One possible interpretation of electrical microstimulation in the AGF is that it produces a 'phosphene' (illusory sensory stimulus) at the spatial location encoded by the site of stimulation. However, the observed effects were qualitatively different from those caused by a stronger physical stimulus at the congruent location: Whereas AGF microstimulation produced rightward shifts and narrower transition ranges of CRPs, increasing the physical strength of an RF stimulus has been shown to produce increases in both minimum and maximum firing rates in the CRP in addition to rightward shifts of the CRP, but no narrowing of the transition range (Mysore et al., 2011). Therefore, descending influences from the AGF alter the competition among stimulus representations within the midbrain selection network without having the effects of a phosphene.

Effects of spatially non-congruent AGF microstimulation on the encoding of the highest priority stimulus

To fully understand the effects of endogenous influences on the encoding of competing stimuli across the OT space map, we also explored how descending influences affect stimulus competition when they are directed away from the RF stimulus and toward the competitor. This was accomplished by microstimulating at a site in the AGF that encoded the location of the competitor rather than the RF stimulus, a configuration referred to as "non-aligned microstimulation" (Fig. 2A).

Non-aligned AGF microstimulation also produced two key changes in the CRPs of OTid neurons (Fig. 2BC). First, the CRP shifted leftward to favor the competitor (Fig. 2B,C): a weaker competitor stimulus was now able to suppress responses to the RF stimulus, an effect that was quantified as a decrease in the s_{50} (Wald F-test, $F_{1,5}$=19.6, p=0.007; Experimental Procedures). Second, the transition range of the CRP again narrowed, as occurred with aligned microstimulation, reflecting a sharper transition from maximum to minimum firing rates with increasing strength of the competitor stimulus (Wald F-test, $F_{1,5}$=13.7, p=0.014; Experimental Procedures). Both effects were consistent across a population of OTid neurons (Fig. 2DE and Fig. S2E), and generalized across sensory modalities (Fig. S2A-D,F). Thus, AGF microstimulation that was congruent with the competitor stimulus biased stimulus competition in favor of the competitor, and also produced sharper transitions as a function of relative stimulus strengths. These effects could not have been predicted from the effects of non-aligned AGF microstimulation on OTid responses to single stimuli, reported previously (divisive response suppression (Winkowski and Knudsen, 2008)).

Effects of AGF microstimulation on the ensemble coding of the highest priority stimulus

What are the implications of these effects of AGF microstimulation for information processing by the OTid network? In the context of purely stimulus-driven, exogenous competition, the ensemble representation across the OTid space map is known to convey an explicitly categorical signal of the strongest stimulus (Mysore and Knudsen, 2011): when relative stimulus strength changes so that one stimulus becomes just stronger than the other, the pattern of ensemble activity in the OTid undergoes a categorical shift to continue to signal the stronger stimulus.

We explored the effect of AGF microstimulation on this categorical ensemble code. To this end, we needed to measure neural activity *across* the OTid space map in response to the competition protocol (Fig. 1A). Specifically, we needed to measure the responses of (i) OTid neurons that encoded the RF stimulus (stimulus of fixed strength), as well as those of (ii) OTid neurons that encoded the competitor stimulus (stimulus of varying strength). The former responses have already been measured as shown in Figure 1. To obtain the latter responses, we performed independent experiments in which the stimulus of increasing strength was presented inside the receptive field of OTid neurons, while the stimulus of fixed strength was presented far outside the receptive field (Fig. 3A; this stimulus configuration is a mirror image of the configuration in Fig. 1A). The microstimulation site in the AGF was congruent with the location of the stimulus of fixed strength.

With this new protocol, AGF microstimulation produced two key changes in the response curves consistent with the results presented thus far: (i) a rightward shift of the response curve, indicating that a stronger stimulus inside the receptive field was required to overcome the suppressive effects of the distant stimulus when AGF microstimulation was congruent with the distant stimulus (Fig. 3B), and (ii) a narrowing of the transition range, reflecting a sharper transition from minimum to maximum firing rates with increasing strength of the stimulus inside the receptive field. Both effects were consistent across a population of OTid neurons (Fig. 3C,D, top panels, and Fig. S3B); there were no systematic effects on the minimum or maximum response rates (Fig. 3C,D, bottom panels).

We used these data to obtain an estimate of the ensemble neural code. We constructed a matrix of neural activity that included responses both of the population of neurons that encoded the stimulus of fixed strength (Fig. 3E, left side; data from Fig. 1B-E) and of the population of neurons that encoded the stimulus of varying strength (Fig. 3E, right side; data from Fig. 3B-D; Experimental Procedures). The individual neurons that constituted the ensemble were measured independently and sequentially across experiments. Each row of the activity matrix represents an estimate of the ensemble activity pattern for one particular strength of the variable stimulus, and each column represents the firing rate of one neuron for different stimulus strengths. Two such matrices were constructed, one using data collected without AGF microstimulation (Fig. 3E), and the other with AGF microstimulation (Fig. 3G).

For each matrix, we examined the similarity between ensemble activity patterns for different relative stimulus strengths by computing pair-wise correlations between the rows of the matrix (Fig. 3F,H). The extent to which the ensemble code was categorical was quantified by a “categorization index” (Experimental Procedures; Fig. S3). Briefly, the index is a number that compares the average difference in correlations *between* versus *within* categories. Positive values of the index indicate larger differences between categories than within them; the higher the categorization index, the clearer the separation between the categories.

Comparison of the categorization indices, obtained without and with AGF microstimulation, revealed a tripling of the categorization index resulting from AGF microstimulation (Fig. 3G,H, bottom panels; Experimental Procedures). In addition, AGF microstimulation shifted the ensemble category boundary to favor the stimulus congruent with AGF activation (Fig.

3G,H). Thus, AGF microstimulation not only biased selection by the ensemble code, but by improving the quality of the explicitly encoded category signal (Mysore and Knudsen, 2011), it also enhanced the ability of a downstream decoder to read out the highest priority stimulus from OTid ensemble activity (Gollisch and Meister, 2010).

The improvement in the quality of network-wide categorization with AGF microstimulation is a direct consequence of the narrowing of response transition ranges (Mysore and Knudsen, 2011). These sharper CRP transitions observed at OTid sites, *both* aligned as well as misaligned with the AGF, are qualitatively different from previously reported attentional effects on feature processing in sensory cortical areas (Carrasco, 2011; Maunsell and Treue, 2006; Reynolds and Chelazzi, 2004) that are characterized by improved encoding (higher firing rates and stimulus-feature discriminability) when attention is directed towards the RF (or towards the preferred stimulus), but degraded encoding when attention is directed away from the RF. The sharper response transitions observed at *all* competing locations are appropriate for a network that is involved in generating a selection signal for the highest priority stimulus by comparing activity levels across the entire space map.

Computational modeling of circuit mechanisms underlying effects of AGF microstimulation

The novel finding of network-wide sharpening of competitive response transitions led us to ask: What circuit mechanisms could give rise to these effects of AGF microstimulation on the midbrain selection signal? To address this question, we adopted a first-principles, computational modeling approach. Our model was based on an anatomically grounded circuit, characterized previously (Goddard et al., 2014; Mysore and Knudsen, 2012) (Fig. 4). This circuit consisted of (i) OTid units, (ii) inhibitory units that mediate global, competitive inhibition across the OTid space map (representing neurons in the GABAergic midbrain nucleus Imc (Mysore and Knudsen, 2013; Wang et al., 2004)), and (iii) direct inhibitory feedback among these inhibitory units (Goddard et al., 2014; Mysore and Knudsen, 2012). For simplicity, only 2 spatial channels (representing locations #1 and #2) are shown, but the model readily extends to an arbitrarily large number of spatial channels. We modeled the loom speed-response functions of OTid and Imc neurons as sigmoidal functions (eqn. 1; Experimental Procedures):

$$r = c + \left(\frac{l^n}{l^n + s_{50}^n} \right) \quad (1)$$

where the firing rate response r of a neuron to a stimulus of loom speed l depends on the parameters c, the minimum response, h, the maximum change in response, s_{50}, the loom speed that yields a half-maximum response, and n, a factor that controls response saturation. This equation fits well experimentally observed loom speed–response functions in the OTid (Mysore et al., 2010; Mysore and Knudsen, 2012).

We modeled the inhibition due to Imc activity as divisive inhibition, consistent with experimental findings (Mysore et al., 2010). In the interest of generality, divisive inhibition

was implemented as acting through a combination of both input and output divisive factors (eqn. 2),

$$r=\left(\frac{1}{s_{out}+1}\right)\cdot\left(\frac{c}{s_{in}+1}+\left(\frac{l^n}{l^n+s_{50}^n+s_{in}^n}\right)\right) \quad (2)$$

where s_{in} and s_{out} are input and output divisive influences, respectively. The rationale for using this form of the equation (and its validity) has been described in detail previously (Mysore and Knudsen, 2012). We chose all parameter values in equations (1) and (2) based on experimental measurements and previous work (Experimental Procedures) (Mysore et al., 2011; Mysore and Knudsen, 2012).

Model I—Two experimental findings guided our initial approach to incorporating the influence of AGF microstimulation into the model: first, AGF axons project directly to the OTid (Knudsen et al., 1995); second, aligned AGF microstimulation focally increases the responsiveness of OTid neurons to *single* RF stimuli via multiplicative gain control (Winkowski and Knudsen, 2006, 2008). We, therefore, asked if such direct modulation of the loom speed-response functions of OTid units by descending AGF projections could be sufficient to account for the observed effects of AGF microstimulation on the midbrain selection signal. We modeled multiplicative gain control of OTid responses to single stimuli using equation 3, which, in the interest of generality, allowed for both input and response multiplicative gain modulation. This form of equation 3 is based on published work on multiplicative gain control (Williford and Maunsell, 2006), and is derived from equation 1 by including input and response gain factors, represented by m_{in} and m_{out}, respectively, the two free parameters in the model (Experimental Procedures).

$$r=c+m_{out}\cdot\left(\frac{l^n}{l^n+m_{in}\cdot s_{50}^n}\right) \quad (3)$$

Figure 5A illustrates the space-specific effect of AGF microstimulation on OTid units in the model: the red ring around OTid unit # 1 denotes the site at which AGF microstimulation was chosen to “act”, and the associated inset shows that the nature of this action was multiplicative gain modulation.

Using this model (Experimental Procedures), we simulated the responses of OTid unit #1 to the competition protocol, without and with the influence of aligned AGF microstimulation. OTid unit #1 is the model equivalent of the neurons from which we recorded experimentally under these conditions. In our simulations, we found that aligned AGF microstimulation produced a general increase in the responses for all strengths of the competitor stimulus (Fig. 5B). However, no combination of values of the input and response multiplicative gain parameters could produce either of the key effects of AGF microstimulation on the CRP: neither a rightward shift nor a narrowing of the transition range (Fig 5B,C). The reason for this inability becomes clear upon closer examination of the inputs to OTid unit #1, specifically, its inhibitory input due to the competitor. Because the activity of Imc unit #2,

encoding a location distant from that of the RF stimulus, is unchanged by AGF microstimulation, the inhibition impinging on OTid unit #1 is identical under both conditions. Consequently, the higher level of excitation caused by AGF microstimulation results simply in an upward but not a rightward shift of the CRP (Fig. 5B). Thus, this model indicates that the effects of AGF microstimulation on OTid CRPs cannot be accounted for by just space-specific modulations of the sensory gain of OTid units.

Model II—Based on these results, we hypothesized that in order to account for the two key effects of microstimulation, the inhibitory drive impinging on OTid unit #1 (from Imc unit #2) must also be affected by aligned AGF microstimulation. From a circuit perspective, the simplest way to implement this effect is to have the space-specific AGF signal modulate responses of aligned neurons that are *within* the global inhibitory feedback loop between the competing channels (Figs. 4 and 6A).

To test this hypothesis, we created a second version of the model in which the AGF signal modulated the loom speed-response function of the aligned Imc unit (Fig. 6A: Imc unit #1; AGF action denoted by red ring and inset). Because of the inhibitory feedback that distributes globally among Imc units (Figs. 4, 5A and 6A), a feature that is supported by recent experimental findings (Goddard et al., 2014), AGF-induced modulation of Imc unit #1 in this model also causes modulation of the inhibitory input impinging on OTid unit #1 (from Imc unit #2).

We assumed that AGF modulation of loom speed responses in the Imc was also multiplicative (Fig. 6A, inset). This assumption allowed for direct comparison of the results from this model with the results from the first version of the model (Fig. 5A). Moreover, this assumption is plausible, because of the consistent observation of multiplicative gain control across brain areas and its established use in models of brain computations (Reynolds and Chelazzi, 2004; Williford and Maunsell, 2006). As before, we allowed for both input and response multiplicative gain of single-stimulus, loom speed responses in the Imc (similar to eqn 3).

Using this model (Experimental Procedures), we simulated the responses of OTid unit #1 to the competition protocol, without and with the influence of aligned AGF microstimulation. We found that this model successfully reproduced both of the key effects: rightward shifts of CRPs and a narrowing of transition ranges (Fig. 6B). These effects (Fig. 6C, top panel), along with very modest effects on minimum and maximum response rates (Fig. 6D, top panel), were observed over large ranges of parameter values (Fig. 6C, D bottom panels; Experimental Procedures). The range of percentage-change values observed in our simulations as a function of the values of the free parameters (Figs. 6C and 6D; top panels) captured the variation observed experimentally (Figs. 1 and 2), with the average experimentally-observed values (Figs. 6C and 6D; top panels; colored arrows) falling close to the middle of the range of values from the simulations. These findings demonstrate the robustness of the model.

Not only did this model account successfully for the effects of *aligned* AGF microstimulation, it also simultaneously reproduced the effects of *non-aligned* AGF

microstimulation on OTid CRPs, as shown in Figure. 6E-H. In this configuration, the "site of AGF microstimulation" in the model is non-aligned with the "site of recording" in the OTid, and microstimulation modulates Imc unit activity in a focal, space-specific manner.

Model III—In the interest of completeness, we next tested the effectiveness of a "mixed" model, in which AGF microstimulation modulated loom speed responses in *both* the OTid and the Imc. We found that the mixed model also successfully reproduced the key, experimentally observed effects of aligned as well as non-aligned AGF microstimulation over large ranges of parameter values (Fig. S4 and Supplemental Text).

In summary, by having the AGF activate, in a space-specific manner, units within the globally projecting inhibitory feedback loop, simple, biologically grounded models (II and III) reproduced all of the key effects of AGF microstimulation on the midbrain representation of the highest priority stimulus.

Experimental validation of model predictions

The successful models (models II and II), which involved modulation of feedback inhibition, yielded a strong, testable prediction: that AGF microstimulation must increase the discriminability of the highest priority stimulus, specifically, the d' (the difference in mean responses divided by the product of response variabilities; Experimental Procedures), computed across the category boundary (at s_{50}). Two properties of the model combine to yield this prediction: (i) the feedback inhibition in these models acts to enhance the difference between mean responses to stimulus pairs straddling the category boundary (Fig. 1CE, Fig. S1BD, Fig. 2CE, and Fig. S2BD), and (ii) attractor models, of which models II and III are examples (Machens et al., 2005; Mysore and Knudsen, 2012; Wang, 2008), produce a reduction in the variability of responses near the category boundary (Deco and Hugues, 2012).

We tested this prediction by computing d' with experimentally measured OTid neuronal responses to competing stimulus pairs that just straddled the category boundary, i.e., pairs for which the discrimination of the higher priority stimulus is most difficult. We found that AGF microstimulation (both aligned and non-aligned) indeed caused a substantial increase in d' (Fig. 7 and Fig. S3A). These results demonstrate an improvement in the neural discriminability of the highest priority stimulus across the OTid space map. Moreover, because d' is a metric of the performance of an ideal observer with access just to the activity of OTid neurons, these results independently confirm that AGF microstimulation can substantially improve the ability of a downstream decoder to read out the location of the highest priority stimulus from OTid activity (Fig. 3).

DISCUSSION

Selection signals for attention emanate not only from the midbrain but also from various regions of the forebrain, the prefrontal and posterior parietal cortex in mammals. The interaction of these selection signals determines the information that is attended next (Bisley, 2010; Knudsen, 2012). Past work, examining neural responses in behaving monkeys, has found signatures of target selection in several brain areas, including the FEF, the lateral

intraparietal area (LIP) and the SCid (Bisley and Goldberg, 2003; Kim and Basso, 2008; McPeek and Keller, 2002; Monosov et al., 2008). In each of these areas, subtypes of neurons respond with differentially high response rates when the stimulus inside their spatial receptive field is selected as the target for decision. Computational modeling work has characterized selection in terms of a race-to-bound process or one-dimensional decay process to account for the dynamics of neural responses during selection tasks (Ganguli et al., 2008; Gold and Shadlen, 2007; Smith and Ratcliff, 2004; Wang, 2012). Other models have invoked recurrent interactions along with feedback inhibition (Machens et al., 2005), including the potential contribution of multiple brain areas (Wang, 2008). In addition, probabilistic decoding frameworks have been proposed for reading out selection from neural population activity (Kim and Basso, 2010), and for dissociating selection bias from perceptual sensitivity (Sridharan et al., 2014).

The experiments reported here depart from these previous studies in two key ways. First, the stimulus protocol measured changes in neural responses to parametric changes in the relative strengths of competing stimuli. Therefore, the results were able to elucidate how the representation of the highest priority stimulus changes as competing stimuli become progressively more similar. In addition, they showed that the effects of endogenous influences on the neural representation of the highest priority stimulus are distinct and cannot be predicted from their effects on the representations of single stimuli (Winkowski and Knudsen, 2008). Indeed, they reveal that the midbrain network operates in a different regime when it is encoding the strengths of multiple stimuli of versus the strength of just a single stimulus. When only a single stimulus is present, competitive mechanisms are not engaged and congruent AGF stimulation enhances the representation of the stimulus (Winkowski and Knudsen, 2008). In contrast, when multiple stimuli are present, the OTid represents primarily the strength of a stimulus *relative* to that of all other stimuli, and congruent AGF stimulation biases the competition in favor of it becoming the highest priority stimulus.

Second, the modeling approach, which was based on known functional and anatomical properties of neurons in the circuit, identified a critical circuit mechanism that is essential for generating the distinctive neural representations that we observed experimentally. This mechanism implicates specific circuit motifs in the brain for generating selection signals, implications that can be tested experimentally in future studies.

Rules for the integration of endogenous and exogenous information for stimulus selection

What are the rules by which the brain integrates endogenous and exogenous information to signal the location of the highest priority stimulus? The results reveal three rules that operate in the midbrain selection network.

First, the biasing rule: endogenous influences can shift the balance of competition in the network without dictating it. A competing stimulus that is sufficiently strong can overcome the endogenous bias so that the network selects the location of the more physically salient stimulus over the endogenously specified location. This characteristic is consistent with human psychophysics (Einhauser et al., 2008; Treisman, 1964), monkey psychophysics

(Burrows and Moore, 2009), with our daily experience, and with the recent finding that the location specified by spatial cueing (an endogenous influence) can be dissociated from the location that is selected for driving behavior (Zenon and Krauzlis, 2012).

Second, the discriminability enhancement rule: endogenous influences enhance categorical state-changes in the network resulting in a substantial increase in the ability of a decoder to discriminate the highest priority stimulus, especially when the relative priorities of stimuli are similar. This rule accounts for the profile of behavioral deficits that have been reported in monkeys following inactivation of the SC: increasingly severe deficits in target selection when distracters are progressively more similar to the target (Lovejoy and Krauzlis, 2010; McPeek and Keller, 2004). It also supports the suggestion that attention involves state changes in information processing (Harris and Thiele, 2011).

Third, the customization rule: endogenous influences customize their modulation of network activity depending on the information processing goals of each network. In the mammalian sensory cortex, endogenous influences improve the processing of the *current* target of attention and degrade responses to competing, *currently* unattended stimuli (Carrasco, 2011; Kastner and Ungerleider, 2000; Maunsell and Treue, 2006; Reynolds and Chelazzi, 2004). In contrast, in the midbrain selection network, endogenous influences enhance discriminability across the entire network, thereby improving the ability of the network to distinguish the highest priority information as the potential *upcoming* target of attention.

Neural mechanisms for implementing rules of selection

Our findings provide the first mechanistic insights into the neural implementation of the rules described above. Endogenous modulation of feedback inhibition among competing information channels emerged as a necessary underlying mechanism. The particular implementation employed in our model, of *direct* gain modulation of aligned inhibitory units in a topographically organized, globally inhibitory circuit, represents one possible alternative; direct anatomical projections from the AGF to the Imc that could support this alternative are yet to be discovered. Alternative implementations that accomplish the same effects, but do so less efficiently, involve pathways from the AGF to the Imc through greater numbers of intermediate synapses. Two such indirect pathways have been described. One is via neurons in layer 10 of the OT (OT_{10}; Knudsen et al, 1995) that provide direct input to the Imc (Wang et al., 2004). Another pathway is via cholinergic neurons in the midbrain tegmental nucleus, the Ipc (Wang et al., 2006). Ipc neurons project to the OT in a space-specific manner and are thought to recurrently amplify OT activity (Marin et al., 2005). AGF activation of the Ipc (Knudsen et al., 1995) could modulate OT_{10} responses and, subsequently, Imc responses. These alternative implementations of the mechanism are not mutually exclusive, and their involvement and relative importance in mediating AGF effects remain to be determined.

The anatomical pathways and circuit mechanism of selection identified here generalize across animal species and brain areas. Analogs of the GABAergic and cholinergic circuits in the midbrain network are found in all classes of vertebrates, reflecting the fundamental importance of these circuits and the computations they perform (Knudsen, 2011). In addition, long-range inhibition and reciprocally inhibitory loops have been identified in

several major cortical and subcortical brain areas (Bolzon et al., 2009; Deleuze and Huguenard, 2006; Falkner et al., 2010; Haider et al., 2013; Hull and Regehr, 2012; McDonald and Burkhalter, 1993; Melzer et al., 2012; Picardo et al., 2011), and the functional importance of competitive inhibition for attention has been demonstrated in humans (Gazzaley et al., 2005). Therefore, we propose that the mechanism of gain modulation of feedback inhibition among competing channels is implemented widely for endogenous regulation of selection circuits. Operating in both midbrain and forebrain attention networks, this mechanism could generate selection signals that combine to control the next locus of spatial attention.

EXPERIMENTAL PROCEDURES

Animals

Experiments were performed on 8 head-fixed, non-anesthetized, adult barn owls (*Tyto alba*). Both male and female birds were used. All procedures for bird care and use were approved by the Stanford University Institutional Animal Care and Use Committee and were in accordance with the National Institutes of Health and the Society for Neuroscience guidelines for the care and use of laboratory animals.

Neurophysiology

Experiments were performed following protocols that have been described previously (Mysore et al., 2010, 2011; Mysore and Knudsen, 2013). Briefly, epoxy-coated tungsten microelectrodes (AM Systems, 250μm diameter, 1-5 MΩ at 1 kHz) were used to record single and multi-units extracellularly. Animals were briefly anesthetized with a mixture of isofluorane (1.5-2%) and nitrous oxide/oxygen (45:55 by volume) at the start of the experiment in order to secure them in the experimental rig. Isofluorane and nitrous oxide were subsequently was turned off and recordings were made in animals that were not anesthetized (Supplemental Experimental Procedures). All recordings in the optic tectum were made in layers 11-13 of the optic tectum (OTid).

AGF microstimulation

Electrical microstimulation of the arcopallial gaze field (AGF) followed the protocol utilized previously (Mysore and Knudsen, 2013; Winkowski and Knudsen, 2006) and described in detail in Supplemental Experimental Procedures. Briefly, an epoxy-coated tungsten microelectrode (FHC; 1 MΩ at 1kHz) was used deliver biphasic 200 Hz pulses for 25 ms in the AGF (Grass S88 stimulator with two Grass stimulus isolation units PSIU-6). AGF stimulation was typically delivered starting at 0 ms (i.e., simultaneously with stimulus onset); it was delivered starting at -25 ms (25 ms before stimulus onset) if the stimulus congruent with the AGF stimulation was an auditory stimulus (Mysore and Knudsen, 2013; Winkowski and Knudsen, 2006). Current levels used (5-25 μA) were far below those required to elicit small amplitude eye deflections (100-600 μA).

Site selection for recording and analysis

“Valid” OTid sites were defined as those at which AGF microstimulation produced an effect on spatial tuning curves (Winkowski and Knudsen, 2008) measured with single, looming

visual stimuli. Competitor strength-response profiles or CRPs were measured only at valid sites,. Multi-unit spike waveforms from a valid recording site were sorted off-line into putative single units (“neurons”), as described previously (Mysore et al., 2011).

Sensory stimuli

Visual and auditory stimuli used here have been described previously (Mysore et al., 2010, 2011). Briefly, looming visual stimuli were presented on a tangent screen in front of the owl. They were dots that expanded linearly in size over time, starting from a size of 0.6° in radius. The strength (physical salience) of a looming stimulus was controlled by its loom speed.

Auditory stimuli, delivered dichotically through matched earphones, were presented as though from different locations by filtering sounds with head-related transfer functions (Witten et al., 2010). The strength of an auditory stimulus was controlled by its average binaural level. The range of binaural levels tested was within 0 to 50 dB relative to unit threshold (Mysore et al., 2010, 2011).

Stimulus presentations without and with AGF microstimulation were always randomly interleaved, with between 10 -15 repetitions in each condition.

The RF and competitor stimuli were presented so that they always occurred within the same hemifield. The relative locations of the RF stimulus, competitor, and the location encoded by the site of electrical microstimulation for all the experiments are plotted in Figs. S1E-F, S2E-F, and S3.

Data analysis and statistical methods

All analyses were carried out with custom MATLAB code as described previously (Mysore et al., 2011; Mysore and Knudsen, 2011, 2013). Briefly, the spatial receptive field for each neuron was defined as the set of locations at which a single stimulus evoked responses above baseline. Response firing rates were computed by counting spikes over a 200 ms time window (median duration; 95 % CI of [200 ms, 225 ms]), starting at 100 ms after stimulus onset (median starting time; 95 % CI of [75 ms, 100 ms]), and converting the resulting count into spikes per second.

CRP responses of neurons from valid sites were tested for correlation with the strength of the competitor stimulus (Spearman's rank correlation coefficient), and only those that showed significant correlation ($p<0.05$) were included in subsequent analysis (see Supplemental Experimental Procedures).

Ensemble code—To construct an estimate of the OTid ensemble code, we adopted an approach utilized in previous reports (Mysore and Knudsen, 2011; Niessing and Friedrich, 2010) and described in detail in Supplemental Experimental Procedures.

Categorization index—The quality of categorization by the ensemble code was quantified using a *categorization index* (Freedman and Assad, 2006; Mysore and Knudsen, 2011) that compared two metrics: (i) the average within-category difference in response

correlations (WCD), and (ii) the average between-category difference in response correlations (BCD). The categorization index was defined as (BCDWCD)/(BCD+WCD), with positive values of the index indicating larger differences between categories than within a category, and thereby revealing a categorical representation, and negative values of the index indicating smaller differences between categories than within a category. WCD and BCD values were calculated as described previously (Freedman and Assad, 2006; Mysore and Knudsen, 2011); see Supplemental Experimental Procedures and Figure S3 for details.

Discriminability

Discriminability was computed using the metric d', defined for the distributions of responses to two stimulus conditions, as $(m_1 - m_2)/\sqrt{(s_1 * s_2)}$, where m_1 and m_2 are the means, and s_1 and s_2, the standard deviations, of the two sampled distributions.

Statistical testing—Parametric or non-parametric, paired statistical tests were applied based on whether the distributions being compared were Gaussian or not (Lilliefors test of normality); tests were two-tailed. The Holm-Bonferroni correction for multiple comparisons was applied when appropriate. Data shown as a ± b refer to mean ± s.e.m. The '*' symbol indicates significance at the 0.05 level.

To test whether AGF microstimulation had a statistically significant effect on the parameters of the CRP, we used the Wald F-test (see Supplemental Experimental Procedures).

Computational modeling

The values of the four parameters in the sigmoid describing the single stimulus loom speed-response functions for OTid and Imc units (eqn. 1 in the text) were chosen as follows. For OTid units, c=5.3, h=22.2, s_{50}=11.6, m=2; the resulting equation yielded the best sigmoidal fit to the experimentally measured, average loom speed-response function (Mysore and Knudsen, 2012). For Imc units, c=5, h=15, s_{50}=8, m=3, based on published work (Mysore and Knudsen, 2012).

The divisive inhibitory effect of the Imc on the responses of OTid neurons, and the reciprocal inhibitory connectivity between Imc neurons, were modeled as described previously (Mysore and Knudsen, 2012); key details are highlighted in Supplemental Experimental Procedures.

Gain control of OTid (and Imc) responses by aligned AGF microstimulation were modeled as a combination of input and response multiplication of the single-stimulus, loom speed-response functions (eqn. 3 in the text), following published work (Williford and Maunsell, 2006; Winkowski and Knudsen, 2008). In this equation, m_{in} and m_{out} are free parameters of the model, representing input and response multiplicative gain, respectively, with m_{in} taking values ≤1 (m_{in}=1 represents no input multiplicative influence, lower m_{in} values represent more powerful input multiplication), and m_{out} taking values ≥1 (m_{out}=1 represents no response multiplicative influence; higher m_{out} values represent more powerful response multiplication).

For the simulations in Figures 5 and 6, m_{in} values were varied over [0.25,1], and m_{out} values were varied over [1,2.1] These ranges were chosen because they were more than wide enough, respectively, to account for the experimentally reported leftward shifts, and increases in the maximum firing rates, of single stimulus-response functions in the OTid following aligned AGF microstimulation (Winkowski and Knudsen, 2008); see Supplemental Experimental Procedures. The same ranges of m_{in} and m_{out} values were used to test the effects of both AGF→ OTid and AGF→ Imc gain modulation in simulations.

Supplementary Material

Refer to Web version on PubMed Central for supplementary material.

Acknowledgements

This work was supported by funding from the NIH (9R01 EY019179, EIK). We are grateful to Ali Asadollahi, Astra Bryant, Alex Goddard, and Jason Schwarz for critically reading the manuscript.

REFERENCES

Armstrong KM, Moore T. Rapid Enhancement of Visual Cortical Response Discriminability by Microstimulation of the Frontal Eye Field. Proc Natl Acad Sci USA. 2007; 104:9499–9504. [PubMed: 17517599]

Asadollahi A, Mysore SP, Knudsen EI. Stimulus-driven competition in a cholinergic midbrain nucleus. Nat Neurosci. 2010; 13:889–895. [PubMed: 20526331]

Bisley JW. The neural basis of visual attention. J Physiol. 2010; 589:49–57. [PubMed: 20807786]

Bisley JW, Goldberg ME. Neuronal activity in the lateral intraparietal area and spatial attention. Science. 2003; 299:81–86. [PubMed: 12511644]

Bolzon DM, Nordstrom K, O'Carroll DC. Local and large-range inhibition in feature detection. J Neurosci. 2009; 29:14143–14150. [PubMed: 19906963]

Bruce CJ, Goldberg ME, Bushnell MC, Stanton GB. Primate frontal eye fields. II. Physiological and anatomical correlates of electrically evoked eye movements. J Neurophysiol. 1985; 54:714–734. [PubMed: 4045546]

Burrows BE, Moore T. Influence and limitations of popout in the selection of salient visual stimuli by area V4 neurons. J Neurosci. 2009; 29:15169–15177. [PubMed: 19955369]

Carello CD, Krauzlis RJ. Manipulating intent: evidence for a causal role of the superior colliculus in target selection. Neuron. 2004; 43:575–583. [PubMed: 15312655]

Carrasco M. Visual attention: the past 25 years. Vision Res. 2011; 51:1484–1525. [PubMed: 21549742]

Cavanaugh J, Wurtz RH. Subcortical modulation of attention counters change blindness. J Neurosci. 2004; 24:11236–11243. [PubMed: 15601929]

Clark KL, Armstrong KM, Moore T. Probing neural circuitry and function with electrical microstimulation. Proceedings Biological sciences / The Royal Society. 2011; 278:1121–1130. [PubMed: 21247952]

Deco G, Hugues E. Neural network mechanisms underlying stimulus driven variability reduction. PLoS Comput Biol. 2012; 8:e1002395. [PubMed: 22479168]

Deleuze C, Huguenard JR. Distinct electrical and chemical connectivity maps in the thalamic reticular nucleus: potential roles in synchronization and sensation. J Neurosci. 2006; 26:8633–8645. [PubMed: 16914689]

Deubel H, Schneider WX. Saccade target selection and object recognition: evidence for a common attentional mechanism. Vision Res. 1996; 36:1827–1837. [PubMed: 8759451]

Dias EC, Segraves MA. Muscimol-induced inactivation of monkey frontal eye field: effects on visually and memory-guided saccades. J Neurophysiol. 1999; 81:2191–2214. [PubMed: 10322059]

Einhauser W, Rutishauser U, Koch C. Task-demands can immediately reverse the effects of sensory-driven saliency in complex visual stimuli. J Vis. 2008; 8:2, 1–19. [PubMed: 18318628]

Falkner AL, Krishna BS, Goldberg ME. Surround suppression sharpens the priority map in the lateral intraparietal area. J Neurosci. 2010; 30:12787–12797. [PubMed: 20861383]

Freedman DJ, Assad JA. Experience-dependent representation of visual categories in parietal cortex. Nature. 2006; 443:85–88. [PubMed: 16936716]

Ganguli S, Bisley JW, Roitman JD, Shadlen MN, Goldberg ME, Miller KD. One-dimensional dynamics of attention and decision making in LIP. Neuron. 2008; 58:15–25. [PubMed: 18400159]

Gazzaley A, Cooney JW, McEvoy K, Knight RT, D'Esposito M. Top-down enhancement and suppression of the magnitude and speed of neural activity. J Cogn Neurosci. 2005; 17:507–517. [PubMed: 15814009]

Goddard CA, Mysore SP, Bryant AS, Huguenard JR, Knudsen EI. Spatially Reciprocal Inhibition of Inhibition within a Stimulus Selection Network in the Avian Midbrain. PLoS One. 2014; 9:e85865. [PubMed: 24465755]

Gold JI, Shadlen MN. The neural basis of decision making. Annu Rev Neurosci. 2007; 30:535–574. [PubMed: 17600525]

Goldberg ME, Wurtz RH. Activity of superior colliculus in behaving monkey. II. Effect of attention on neuronal responses. J Neurophysiol. 1972; 35:560–574. [PubMed: 4624740]

Gollisch T, Meister M. Eye smarter than scientists believed: neural computations in circuits of the retina. Neuron. 2010; 65:150–164. [PubMed: 20152123]

Haider B, Hausser M, Carandini M. Inhibition dominates sensory responses in the awake cortex. Nature. 2013; 493:97–100. [PubMed: 23172139]

Harris KD, Thiele A. Cortical state and attention. Nat Rev Neurosci. 2011; 12:509–523. [PubMed: 21829219]

Hoffman JE, Subramaniam B. The role of visual attention in saccadic eye movements. Percept Psychophys. 1995; 57:787–795. [PubMed: 7651803]

Horwitz GD, Newsome WT. Separate signals for target selection and movement specification in the superior colliculus. Science. 1999; 284:1158–1161. [PubMed: 10325224]

Hull C, Regehr WG. Identification of an inhibitory circuit that regulates cerebellar Golgi cell activity. Neuron. 2012; 73:149–158. [PubMed: 22243753]

Ignashchenkova A, Dicke PW, Haarmeier T, Thier P. Neuron-specific contribution of the superior colliculus to overt and covert shifts of attention. Nat Neurosci. 2004; 7:56–64. [PubMed: 14699418]

Kastner S, Ungerleider LG. Mechanisms of visual attention in the human cortex. Annu Rev Neurosci. 2000; 23:315–341. [PubMed: 10845067]

Kim B, Basso MA. Saccade target selection in the superior colliculus: a signal detection theory approach. J Neurosci. 2008; 28:2991–3007. [PubMed: 18354003]

Kim B, Basso MA. A probabilistic strategy for understanding action selection. J Neurosci. 2010; 30:2340–2355. [PubMed: 20147560]

Knudsen EI. Control from below: the role of a midbrain network in spatial attention. Eur J Neurosci. 2011; 33:1961–1972. [PubMed: 21645092]

Knudsen, EI. Midbrain and forebrain systems for bottom-up control of spatial attention.. In: Mangun, GR., editor. Neuroscience of attention: attention control and selection. Oxford University Press; New York: 2012.

Knudsen EI, Cohen YE, Masino T. Characterization of a forebrain gaze field in the archistriatum of the barn owl: microstimulation and anatomical connections. J Neurosci. 1995; 15:5139–5151. [PubMed: 7623141]

Knudsen EI, Knudsen PF. Disruption of auditory spatial working memory by inactivation of the forebrain archistriatum in barn owls. Nature. 1996; 383:428–431. [PubMed: 8837773]

Kowler E, Anderson E, Dosher B, Blaser E. The role of attention in the programming of saccades. Vision Res. 1995; 35:1897–1916. [PubMed: 7660596]

Li B, Wang L, Wang Y, Diao Y. Orientational and directional selectivities of visual neurons in the superior colliculus of the cat. Sci China C Life Sci. 1996; 39:123–132. [PubMed: 8760460]

Lovejoy LP, Krauzlis RJ. Inactivation of primate superior colliculus impairs covert selection of signals for perceptual judgments. Nat Neurosci. 2010; 13:261–266. [PubMed: 20023651]

Machens CK, Romo R, Brody CD. Flexible control of mutual inhibition: a neural model of two-interval discrimination. Science. 2005; 307:1121–1124. [PubMed: 15718474]

Marin G, Mpodozis J, Sentis E, Ossandon T, Letelier JC. Oscillatory bursts in the optic tectum of birds represent re-entrant signals from the nucleus isthmi pars parvocellularis. J Neurosci. 2005; 25:7081–7089. [PubMed: 16049185]

Maunsell JH, Treue S. Feature-based attention in visual cortex. Trends Neurosci. 2006; 29:317–322. [PubMed: 16697058]

McDonald CT, Burkhalter A. Organization of long-range inhibitory connections with rat visual cortex. J Neurosci. 1993; 13:768–781. [PubMed: 7678860]

McPeek RM, Keller EL. Saccade target selection in the superior colliculus during a visual search task. J Neurophysiol. 2002; 88:2019–2034. [PubMed: 12364525]

McPeek RM, Keller EL. Deficits in saccade target selection after inactivation of superior colliculus. Nat Neurosci. 2004; 7:757–763. [PubMed: 15195099]

Melzer S, Michael M, Caputi A, Eliava M, Fuchs EC, Whittington MA, Monyer H. Long-range-projecting GABAergic neurons modulate inhibition in hippocampus and entorhinal cortex. Science. 2012; 335:1506–1510. [PubMed: 22442486]

Monosov IE, Trageser JC, Thompson KG. Measurements of simultaneously recorded spiking activity and local field potentials suggest that spatial selection emerges in the frontal eye field. Neuron. 2008; 57:614–625. [PubMed: 18304489]

Moore T, Armstrong KM. Selective gating of visual signals by microstimulation of frontal cortex. Nature. 2003; 421:370–373. [PubMed: 12540901]

Moore T, Fallah M. Control of eye movements and spatial attention. Proc Natl Acad Sci U S A. 2001; 98:1273–1276. [PubMed: 11158629]

Muller JR, Philiastides MG, Newsome WT. Microstimulation of the superior colliculus focuses attention without moving the eyes. Proc Natl Acad Sci U S A. 2005; 102:524–529. [PubMed: 15601760]

Mysore SP, Asadollahi A, Knudsen EI. Global inhibition and stimulus competition in the owl optic tectum. J Neurosci. 2010; 30:1727–1738. [PubMed: 20130182]

Mysore SP, Asadollahi A, Knudsen EI. Signaling of the strongest stimulus in the owl optic tectum. J Neurosci. 2011; 31:5186–5196. [PubMed: 21471353]

Mysore SP, Knudsen EI. Flexible categorization of relative stimulus strength by the optic tectum. J Neurosci. 2011; 31:7745–7752. [PubMed: 21613487]

Mysore SP, Knudsen EI. Reciprocal inhibition of inhibition: a circuit motif for flexible categorization in stimulus selection. Neuron. 2012; 73:193–205. [PubMed: 22243757]

Mysore SP, Knudsen EI. A shared inhibitory circuit for both exogenous and endogenous control of stimulus selection. Nat Neurosci. 2013; 16:473–478. [PubMed: 23475112]

Niessing J, Friedrich RW. Olfactory pattern classification by discrete neuronal network states. Nature. 2010; 465:47–52. [PubMed: 20393466]

Picardo MA, Guigue P, Bonifazi P, Batista-Brito R, Allene C, Ribas A, Fishell G, Baude A, Cossart R. Pioneer GABA Cells Comprise a Subpopulation of Hub Neurons in the Developing Hippocampus. Neuron. 2011; 71:695–709. [PubMed: 21867885]

Reynolds JH, Chelazzi L. Attentional modulation of visual processing. Annu Rev Neurosci. 2004; 27:611–647. [PubMed: 15217345]

Smith PL, Ratcliff R. Psychology and neurobiology of simple decisions. Trends Neurosci. 2004; 27:161–168. [PubMed: 15036882]

Sridharan D, Steinmetz NA, Moore T, Knudsen EI. Distinguishing bias from sensitivity effects in multialternative detection tasks. Journal of Vision. 2014 in press.

Stanton GB, Goldberg ME, Bruce CJ. Frontal eye field efferents in the macaque monkey: II. Topography of terminal fields in midbrain and pons. J Comp Neurol. 1988; 271:493–506. [PubMed: 2454971]

Treisman AM. Selective Attention in Man. Br Med Bull. 1964; 20:12–16. [PubMed: 14104089]

Wallace MT, Stein BE. Sensory organization of the superior colliculus in cat and monkey. Prog Brain Res. 1996; 112:301–311. [PubMed: 8979837]

Wang XJ. Decision making in recurrent neuronal circuits. Neuron. 2008; 60:215–234. [PubMed: 18957215]

Wang XJ. Neural dynamics and circuit mechanisms of decision-making. Curr Opin Neurobiol. 2012; 22:1039–1046. [PubMed: 23026743]

Wang Y, Luksch H, Brecha NC, Karten HJ. Columnar projections from the cholinergic nucleus isthmi to the optic tectum in chicks (Gallus gallus): a possible substrate for synchronizing tectal channels. J Comp Neurol. 2006; 494:7–35. [PubMed: 16304683]

Wang Y, Major DE, Karten HJ. Morphology and connections of nucleus isthmi pars magnocellularis in chicks (Gallus gallus). J Comp Neurol. 2004; 469:275–297. [PubMed: 14694539]

Williford T, Maunsell JH. Effects of spatial attention on contrast response functions in macaque area V4. J Neurophysiol. 2006; 96:40–54. [PubMed: 16772516]

Winkowski DE, Knudsen EI. Top-down gain control of the auditory space map by gaze control circuitry in the barn owl. Nature. 2006; 439:336–339. [PubMed: 16421572]

Winkowski DE, Knudsen EI. Distinct mechanisms for top-down control of neural gain and sensitivity in the owl optic tectum. Neuron. 2008; 60:698–708. [PubMed: 19038225]

Witten IB, Knudsen PF, Knudsen EI. A dominance hierarchy of auditory spatial cues in barn owls. PLoS One. 2010; 5:e10396. [PubMed: 20442852]

Wurtz RH, Albano JE. Visual-motor function of the primate superior colliculus. Annu Rev Neurosci. 1980; 3:189–226. [PubMed: 6774653]

Zenon A, Krauzlis RJ. Attention deficits without cortical neuronal deficits. Nature. 2012; 489:434–437. [PubMed: 22972195]

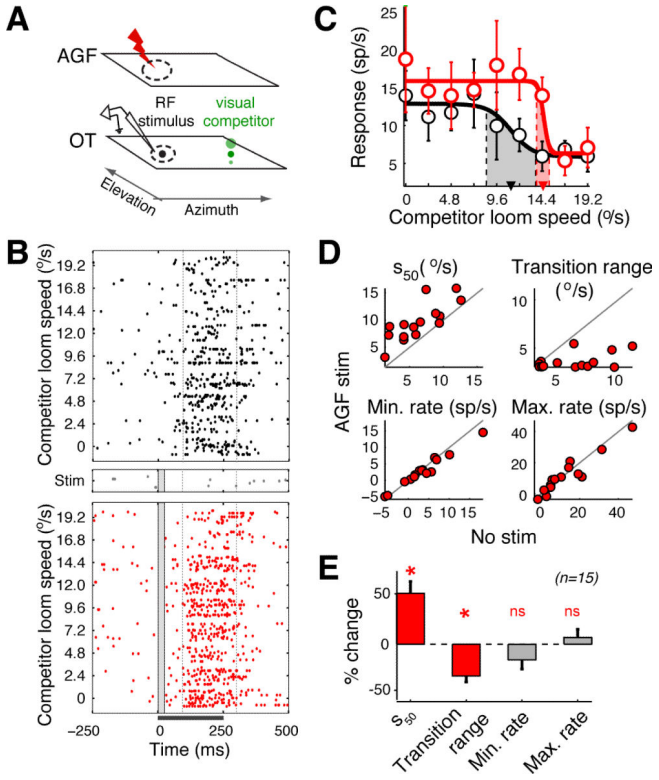

Figure 1. Effects of spatially congruent AGF microstimulation on the encoding of the highest priority stimulus

(A) Schematic of experimental protocol. Illustrated are the representations of space in the OTid and AGF, receptive fields (dashed ovals), electrodes in the OTid (recording icon) and AGF (red lightning bolt), and visual stimuli (black and green dots); both stimuli were presented in the same hemifield. Size of dot: strength (loom speed) of stimulus. (B) Rasters of spike responses of an OTid neuron to the competition protocol without (top panel) and with spatially aligned AGF microstimulation (bottom panel). Also shown are responses to microstimulation alone, delivered in the absence of sensory stimuli (middle panel). Bar underneath the x-axis represents the time of stimulus presentation; vertical box within raster plot indicates the onset and duration of AGF microstimulation. Dashed vertical lines indicate the time window (100-300 ms) during which response firing rates were measured. Distance between the centers of OTid and AGF RFs = 5°; loom speed (strength) of RF stimulus = 10.4°/s; strength of microstimulation current = 20 μA. (C) CRPs without (black) and with (red) aligned AGF microstimulation; computed from the rasters in B. Solid lines: best sigmoidal fits to CRPs; arrowheads: s_{50}; shaded areas: transition ranges. RF stimulus strength = 10.4°/s. Data represent mean ± s.e.m. (D) Scatter plots of values of sigmoidal parameters without vs. with aligned AGF microstimulation. Circles: individual neurons; n=15 neurons from 3 birds. Grey line: line of equality. Average distance between the centers of OTid and AGF RFs = 5° ± 0.8°; average distance between OTid RF center and competitor location = 35° ± 1.2°; Fig. S1E. Average strength of the RF stimulus = 6.9 °/s ± 0.5 °/s; average strength of microstimulation current =13.5 ± 1.3 μA; data: mean ± s.e.m. (E) Population summary of the effects of aligned AGF microstimulation on the parameters of the CRP. '*': $p<0.05$, 'ns': not significant. S_{50}: Wilcoxon signed rank test ("rank-test"),

$p<10^{-3}$, signed rank = 1; transition range: rank-test, $p<10^{-3}$, signed rank =1; minimum rate: t-test, p=0.29, t_{14}=1.12; maximum rate: t-test, p= 0.81, t_{14}=0.24). Data: mean ± s.e.m. See also Figure S1.

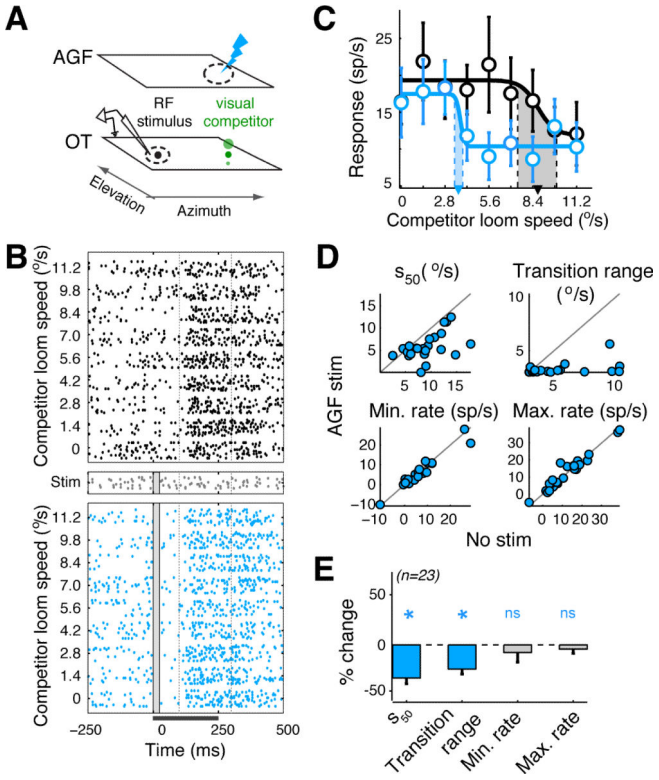

Figure 2. Effects of spatially non-congruent AGF microstimulation on the encoding of the highest priority stimulus

(A-E) Same conventions as in Figure 1. (A) Blue lightning bolt: AGF microstimulation non-aligned with OTid RF but aligned with location of competitor stimulus. (B) Rasters of spike responses of an OTid neuron to the competition protocol without (top panel) and with spatially non-congruent AGF microstimulation (bottom panel). Distance between OTid RF center and AGF RF center/location of competitor = 28.9°; loom speed (strength) of RF stimulus = 4.8°/s; strength of microstimulation current = 10 μA. (C) CRPs without (black) and with (blue) non-aligned AGF microstimulation; computed from the rasters in B. (D) Scatter plots of values of sigmoidal parameters without vs. with non-aligned AGF microstimulation. Circles: individual neurons; n=23 neurons from 7 birds. Average distance between OTid RF center and AGF RF center/ location of competitor = 37.3° ± 3.3; Fig. S2E. Average strength of the RF stimulus = 7.7 °/s ± 0.35 °/s; average strength of microstimulation current =16.5 ± 0.7 μA; data: mean ± s.e.m. (E) Population summary of the effects of aligned AGF microstimulation on the parameters of the CRP. S_{50}: t-test, $p<10^{-3}$, t_{22} = -4.55; transition range: t-test, $p<10^{-3}$, t_{22} = -4.83; minimum rate: rank-test, p=0.93, signed rank = 135; maximum rate: rank-test, p= 0.78, signed rank = 129. Data: mean ± s.e.m.

See also Figure S2.

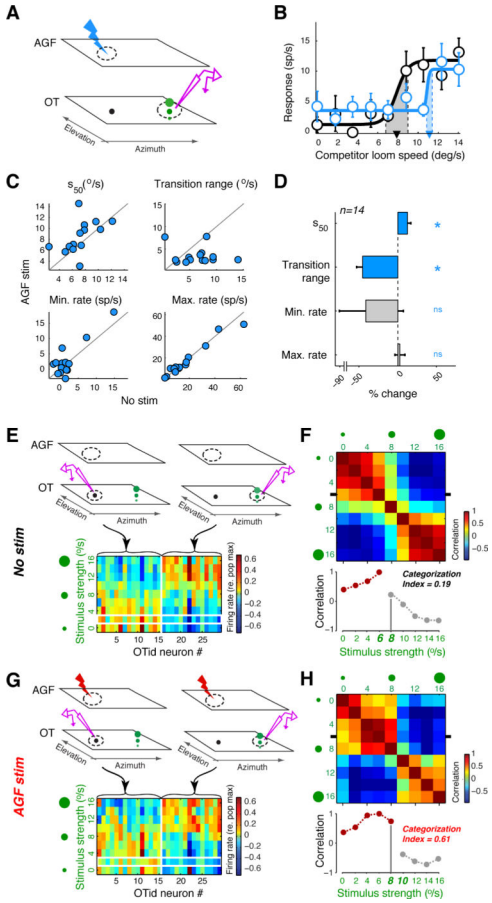

Figure 3. Effects of AGF microstimulation on the ensemble coding of the highest priority stimulus in the OTid

(A-D) Responses of OTid neurons that encode the competitor stimulus in the competition protocol in Figure 1A. Same conventions as in Figure 1. (A) Schematic of the experimental protocol. Configuration of the sensory stimuli is a mirror image of the configuration in Figure 1A. The microstimulation site in the AGF continues to encode the location of the stimulus of fixed strength (as in Figure 1A). (B) Responses of an OTid neuron without (black) and with (blue) AGF microstimulation; strength of the fixed-strength stimulus= 7 °/s. (C) Scatter plots of values of sigmoidal parameters without vs. with AGF microstimulation. (D) Population summary (14 neurons from 5 birds). Data represent mean ± s.e.m. '*': $p<0.05$, 'ns': not significant (s_{50}: rank-test, $p=0.017$, signed rank=15; transition range: rank-test, $p<10^{-3}$, signed rank = 4; minimum rate: rank-test, $p=0.58$, signed rank = 43; maximum rate: $p= 0.32$, t-test, $t_{13}=1.03$).

(E-H) Effect of AGF microstimulation on the OTid ensemble code **(E,F)** OTid ensemble code in the absence of AGF microstimulation. (E) *Top, left:* Schematic illustrating measurement of responses of OTid neurons that encoded the RF stimulus (recording icon highlighted in purple). *Top, right:* Schematic illustrating measurement of responses of OTid neurons that encoded the competitor stimulus. *Bottom:* Matrix of ensemble OTid activity constructed from responses of neurons encoding the RF stimulus (n=15) and those of neurons encoding the competitor stimulus (n=14; panels A-D; Experimental Procedures). Columns = neurons; rows = strengths of the competitor stimulus. (F) *Top*: Matrix of

pairwise correlations (Pearson) between rows of the activity matrix in E. *Bottom*: Horizontal transect through the correlation matrix at the position indicated by the tick marks in the top panel. X-axis labels = competitor strengths. Population category boundary is indicated by the abrupt transition seen between the competitor strengths of 6 °/s and 8 °/s (near the RF stimulus strength of 7.2 °/s; Experimental Procedures). Brown and grey data: the two categories; vertical grey line aids visualization of the right-shifting boundary (compare with H, bottom panel). Categorization index (Mysore and Knudsen, 2011) represents the quality of categorization (Experimental Procedures; Fig. S3). **(G,H)** OTid ensemble code in the presence of space-specific AGF microstimulation (data for each neuron in a and b obtained in a randomly interleaved manner). Same conventions as in E,F.

(H) Population category boundary is shifted over to the right relative to the boundary in F, occurring now between competitor strengths of 8°/s and 10°/s.

See also Figure S3.

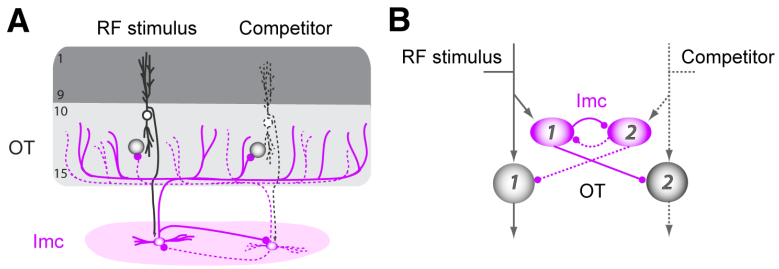

Figure 4. Anatomically grounded circuit model

(**A**) Schematic of anatomical connectivity between the OT and Imc (Goddard et al., 2014; Wang et al., 2004). Shaded circles: OT neurons; purple ovals: Imc neurons. Two spatial channels (#1 and #2) are shown; one of them is represented with dashed lines for visual clarity. **(B)** Schematic of model circuit that respects the anatomy. Shaded circles: OT units; purple ovals: Imc units. Arrows: excitatory connections; lines with spherical heads: inhibitory connections.

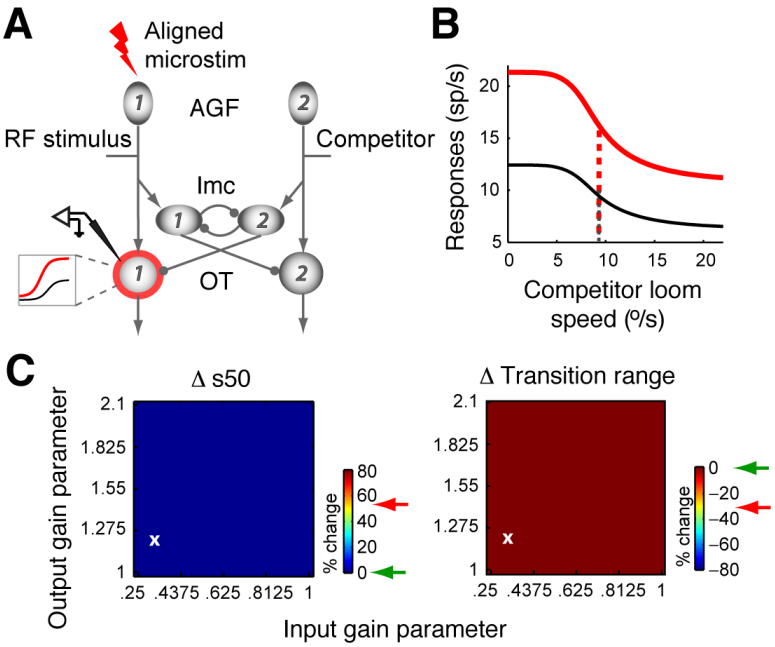

Figure 5. Computational model I: Gain modulation of units outside of the inhibitory feedback loop does not reproduce the experimental effects of AGF microstimulation

The AGF modulates the gain of OTid units in a space-specific manner. **(A-C)** Effects of aligned AGF stimulation. (A) Red ring: OTid unit whose gain is multiplicatively modified (as shown in inset) by aligned AGF microstimulation. Inset: Visual mnemonic illustrating multiplicative gain modulation of OTid responses by AGF microstimulation. Shown are schematic responses of an OTid unit to a single stimulus inside the RF, without (black) and with (red) microstimulation. X-axis, strength of RF stimulus; y-axis, firing rate. (B) Simulated responses for OTid unit #1 without and with AGF stimulation; AGF→OTid input gain parameter = 0.325, response gain parameter = 1.22; values chosen to show representative results, and correspond to the white 'x' in C. (C) Shift in s_{50} (%; left) and change in transition range (%; right) plotted as a function of input and response gain values (Experimental Procedures). Green arrow: largest magnitude of % change from simulation; red arrow: average % change from experiments.

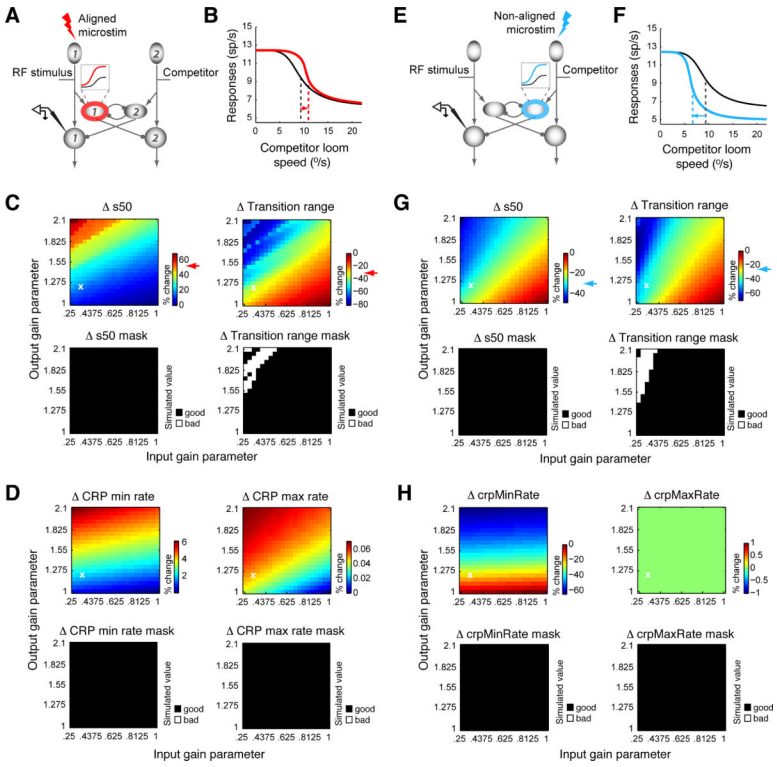

Figure 6. Computational model II: Gain modulation of units inside the inhibitory feedback loop robustly reproduces the experimental effects of AGF microstimulation

The AGF modulates the gain of Imc units in a space-specific manner. Same conventions as in Figure 5. (**A-D**). Effects of aligned AGF stimulation (red icons and data). (A) Inset: Visual mnemonic illustrating multiplicative gain modulation of Imc responses by AGF microstimulation. Shown are schematic responses of an Imc unit to a single stimulus inside the RF, without (black) and with (red) microstimulation. X-axis, strength of RF stimulus; y-axis, firing rate. (B) AGF→Imc input gain parameter = 0.325, response gain parameter = 1.22 (same values as AGF→OTid gain parameters in Figure 5b, and correspond to the white 'x' in C; top panels). (C) *Top panels:* Shift in s_{50} (%; left) and change in transition range (%; right). Red arrow: average % change from experiments (Fig. 1). *Bottom panels:* Plot ("mask") showing whether or not the value of % change in the simulated CRP's s_{50} (left panel) and transition range (right panel) due to AGF microstimulation was within the range of experimentally observed values of % change. Ranges for experimentally observed values were estimated to be the mean ± 2*std, where mean and std were calculated from recordings (Fig. 1E). "Good" (black): simulated values that lie within the range of experimentally observed values; "bad" (white): simulated values that lie outside the range of experimentally observed values. (D) *Top panels:* Change in minimum response rate (%; left) and maximum response rate (%; right) of simulated CRPs. *Bottom panels:* Masks; same conventions as in (C). Range of values of the parameters that yielded results that were consistent with experiments is determined by the area of the intersection of the "good" (black) portions of the four masks from C and D. (**E-H**) Effects of non-aligned stimulation (AGF RF non-aligned with OTid RF, but aligned with location of the competitor; blue icons and data). Same conventions as in (A-D). (F) AGF→Imc input gain parameter = 0.325, response gain

parameter = 1.22. (G) *Top panels*: Blue arrow: average % change from experiments (Fig. 2). *Top-right panel*: No effect of non-aligned AGF microstimulation on the CRP maximum response rate.

See also Figure S4.

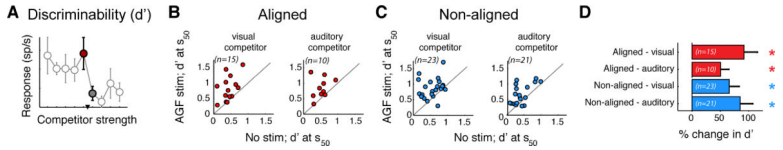

Figure 7. Experimental results validate strong prediction of computational model II

Testing the prediction that AGF microstimulation increases the discriminability of the highest priority stimulus. (**A**) Example CRP (mean ± s.e.m); data straddling CRP category boundary (s_{50}; filled circles) were used to compute d'. (**B-C**) Effect of AGF stimulation on d' calculated from the CRPs of individual OTid neurons. (**D**) Population summaries. '*': $p<0.05$, 'ns': not significant. S_{50}: $p<10^{-3}$, signed rank = 1; transition range: $p=0.004$, signed rank = 1; minimum rate: $p<10^{-3}$, signed rank = 18; maximum rate: $p<10^{-3}$, signed rank = 17; rank-test in all cases). See also Figure S3.